Frontiers in Heat and Mass Transfer

Tech Science Press

Doi:10.32604/fhmt.2025.064444

ARTICLE

Characteristics of Heat Transfer in a Reactive Third-Grade Fluid Flow through Porous Plates with Uniform Suction/Injection

Rajiva Lochan Mohanty, Sumanta Chaudhuri* and Anish Pandey

School of Mechanical Engineering, Kalinga Institute of Industrial Technology, Deemed to be University, Bhubaneswar, 751024, Odisha, India

*Corresponding Author: Sumanta Chaudhuri. Email: sumanta.chaudhurifme@kiit.ac.in

Received: 16 February 2025; Accepted: 09 May 2025; Published: 30 June 2025

ABSTRACT: Characteristics of heat transfer and flow of Newtonian and non-Newtonian fluids through porous walls and in porous media are studied due to their wide range of applications including geothermal reservoirs, heat exchangers, marine propulsion, and aerodynamics. The current study investigates the characteristics of heat transport in a reactive third-grade fluid, moving through permeable parallel plates, with uniform suction/injection velocity. The two permeable, parallel plates are maintained at the same, constant temperature. After being transformed into its dimensionless equivalent, governing equations are solved by employing the Least Squares Method (LSM). The LSM results are further validated with numerical solutions for temperature and velocity. The impact of cross-flow Reynolds number, Peclet number, heat generation parameter, non-Newtonian parameter, and Brinkman number on entropy generation, velocity, temperature, and Bejan number are investigated. The results indicate that temperature distribution is significantly influenced by the third-grade fluid parameter. The maximum temperature drops from almost 0.12 to 0.10 as the third-grade fluid parameter increases from 0.05 to 0.4. When the cross-flow Reynolds number is raised from 0.05 to 3, the maximum temperature drops from 0.12 to around 0.09. Temperature is strongly influenced by the heat generation parameter. A greater understanding of the thermal characteristics necessary for the design of a variety of systems, such as heat exchangers, marine propulsion, aerodynamic systems, etc., may be gained from the findings of the current study.

KEYWORDS: Heat generation; third grade fluids; perturbation method; least square method; uniform suction/injection; porous plates

1 Introduction

The study of heat transfer characteristics in fluid flow through porous media and porous plates has garnered significant interest due to numerous applications [1] in geothermal reservoirs, marine propulsion, heat exchangers, aerodynamics, and other fields. Injection or suction across porous barriers alters velocity, which impacts heat transfer in mass transfer cooling. Fluid velocity distribution is significantly influenced by injection and suction in boundary layer control for wire coating, polymer fiber coating, and film cooling [2]. Due to these host of applications, numerous researchers studied various aspects of heat transfer in porous media and through porous boundaries with combined effects of suction and injection. Mixed convection heat transfer from a vertical porous plate with combined effects of radiation, internal heat generation, and suction/injection was investigated by Jha and Samila [3]. A similarity transformation technique was employed to reduce partial differential equations into ordinary differential equations, which were solved by the shooting technique. Results indicated that radiative heat flux enhanced fluid temperature

and boosted fluid flow. Steady mixed convective flow in a vertical parallel plate channel with combined effects of velocity slip, injection/suction, and temperature jump conditions were examined by Jha and Aina [4]. Exact analytical solutions for momentum and energy conservation equations were obtained and the influence of different parameters on temperature, velocity, heat transfer coefficient, flow rate, and friction coefficient were analyzed. Aly et al. [5] studied coupled heat and mass transfer by unsteady free convection from a vertical plate in a porous medium including the effect of radiation and chemical reaction. Non-dimensional governing equations were numerically solved by explicit finite difference scheme and effects of pertinent parameters on temperature, friction coefficient, and Nusselt number were discussed. Studies of flow through porous plates and media were also conducted for nanofluids [6–8] and Magnetohydrodynamic (MHD) [9,10]. Flow and heat transfer in MHD has numerous applications in nuclear reactor cooling, medical hyperthermia, petroleum engineering, and other fields. MHD natural convection including effects of Joule heating, chemical reaction, and radiation in the vertical porous plate was studied by Chamkha et al. [9]. Governing partial differential equations were solved numerically by a finite difference scheme and the effects of various parameters on linear velocity, temperature, angular velocity, and concentration were analyzed. Chamkha investigated the mixed convection MHD flow in a vertical channel, considering symmetric and asymmetric wall heating scenarios [10]. Effects of heat generation and absorption were considered and analytical solutions for velocity temperature were obtained.

Effects of buoyancy and Navier slip on the rate of generation of entropy in a permeable, vertical channel with uniform suction and injection were investigated by Sudhakar and Balamurugan [11]. Velocity and temperature distribution problems were solved using the perturbation approach. Temperature, velocity, and generation of entropy were examined for variation of injection/suction parameters, cross-flow Reynolds numbers, Brinkman numbers, Peclet numbers, and heat source parameters.

Balamurugan et al. [12] investigated how the same suction/injection velocity in MHD convective flow in a permeable vertical channel affects heat transfer characteristics. Their investigation took into account the impact of velocity slip along the walls. Additionally, the investigation took into account the influence of internal heat generation. Internal heat generation [13] is linked to exothermic chemical reactions or moving fluids where burning occurs. From the obtained analytical solutions, the effects of injection/suction and other factors on temperature, velocity, and generation of entropy were investigated. Analysis of the entropy generation rate aids in estimating various thermal systems' efficiency.

The rate of generation of entropy has been studied by several investigators [14,15] in their study of thermal systems. Das et al. [14] examined the MHD flow of AlO/water nanofluid and Cu-AlO/water hybrid nanofluid across permeable boundaries. The influence of relevant parameters on temperature, velocity, and generation of entropy was investigated, and analytical solutions were obtained. Makinde and Eegunjobi [15] investigated the effects of buoyancy, Brownian motion, thermophoresis, and non-linear thermal radiation on the rate of entropy generation in the flow of a nanofluid down a vertical permeable channel. Using the shooting method and an integration scheme, the governing equations for momentum, energy, and nanoparticle concentration equations were derived and numerically solved. Using the velocity and temperature distribution, the following parameters were examined: skin friction, entropy production rate, Nusselt number, Sherwood number, and Bejan numbers. Numerous other researchers have engaged in research activities related to MHD nanofluids [16–18].

The results of investigations about MHD Newtonian fluids through permeable boundaries were briefly covered in the referred publications above. Studies on nanofluids that use the Newtonian fluid model are also included in this topic. Because of its uses in molten polymers, printing inks, the food products sector, and many other fields, research on electrically conducting non-Newtonian fluids [19–22] through porous plates and media is also growing day by day.

Entropy formation in thermally radiated MHD-driven convective flow of a Casson fluid in a microchannel with a porous medium was investigated by Makinde and Eegunjobi [20]. Entropy generation was investigated about slip, magnetic field, thermal radiation, permeability parameter, and suction/injection. Nusselt number, skin friction, entropy formation, and Bejan number were examined by using the numerical solutions for temperature and velocity. The findings highlighted that the non-Newtonian parameter and magnetic field had a major impact on the results. The mixed convective flow of an electrically conducting Casson fluid was also studied by Eegunjobi and Makinde [21], taking into account the impacts of the following factors: buoyancy force, magnetic field, velocity slip, permeability, injection/suction parameter, thermal radiation absorption, viscosity, and Joule heating. A combination of the fourth-order Runge-Kutta-Fehlbarg integration scheme and the shooting technique was used to numerically solve dimensional governing equations. Analysis was done on how various factors affected temperature, skin friction, velocity, entropy production, Nusselt number, and Bejan number. Mustapha et al. [22] conducted a theoretical and numerical study of thermosolute natural convective heat transfer in Casson nanofluid flow through isotropic porous media with an applied magnetic field. The finite difference approach was used to solve the governing equations, and the effects of different parameters on the concentration and rate of heat transmission were investigated. It was observed that the rate of mass and heat transmission increased when the Casson fluid parameter was raised. Dash and Ojha [23] examined the MHD flow of a viscoelastic fluid between two porous parallel plates with a periodic pressure gradient and a time-varying magnetic field. Analytical solutions for temperature and velocity revealed that backflow is prevented by a low-frequency pressure gradient. Radnia and Nazar [24] examined the impact of injection and suction on heat transport in power-law fluid flow passed a surface (moving). The Runge-Kutta method in conjunction with the shooting approach was used to numerically solve partial differential equations that were reduced to ordinary differential equations. Heat transport was examined about non-Newtonian parameters, injection/suction parameters, and heat source parameters.

Some significant research on porous boundaries and porous media flow of various non-Newtonian fluids was presented in the preceding discussion. It is crucial to remember that the Rivlin-Eriksen fluid of grade three, also known as third-grade fluid [25–27], is a form of non-Newtonian fluid that represents the behavior of different polymers, lubricating oils, and blood flow. Adesanya and Falade [28] conducted research on third-grade fluids using the porous medium. Taking into account the impact of convective cooling, Opanuga et al. [29] investigated the effects of uniform injection/suction on the flow and heat transfer of third-grade fluid flow through porous parallel plates. Temperature and velocity were determined using the Adomian Decomposition Method, and the impacts of various factors on temperature, entropy formation, velocity, and Bejan number were examined.

It is clear from the cited literature that, from a theoretical and practical standpoint, the flow and heat transfer of various non-Newtonian fluids across porous boundaries and media are of great interest. However, there aren't many studies on heat transmission and third-grade fluids flow through porous plates and mediums. In light of this, the current study additionally takes into account the internal heat generation impact while examining third-grade fluid flow through porous plates (parallel) considering uniform injection and suction at the plates. As was previously mentioned, internal heat generation must be taken into account in situations when combustion or exothermic chemical reactions occur in the flow. A real-world application of third-grade fluid through porous plates is in the field of food processing industries. These non-Newtonian fluids display intricate flow behaviors, making them suitable for applications involving heat transfer and thermal management in various appliances such as ovens, fryers, and freezers. In food processing suction/injection are important for efficient heat transfer, flow stability, and product quality. This can help regulate the flow rate, pressure, and temperature and pressure ensuring consistent and efficient

processing conditions. Suction/injection can also improve mixing, blending, and removal of air ensuring product quality.

In this research, the Least-square method (LSM) is applied to solve the non-linear governing equations. Symbolic computing is used to provide semi-analytical solutions. LSM is a semi-analytical approach that combines the features of numerical and analytical transactions. Researchers have utilized LSM to produce high-accuracy expressions for solving non-linear differential equations [25,26]. LSM is used in this work to solve nonlinear differential equations that describe how suction and injection affect third-grade fluid flow through porous plates (parallel) that include an internal heat source. The novelty of the present study is:

- Study of heat transfer (considering convection along cross-flow direction) in third-grade fluid considering temperature-dependent internal heat generation effect and uniform injection and suction through permeable parallel walls. Researchers have already carried out numerous studies on Newtonian fluids, and a substantial body of literature exists on this topic. In stark contrast, when it comes to third-grade fluids, comparable investigations remain notably limited, with only a handful of relevant works available in the open-access literature.
- How field variables like velocity, temperature and entropy generation, Bejan number are affected by non-Newtonian and suction/injection parameters.
- How velocity, temperature, entropy generation, and Bejan number get influenced by heat generation parameter.
- Implementation of LSM for solving non-linear momentum and energy equations for uniform suction and injection. For this type of cross-flow, velocity and temperature profiles are distorted. When selecting base or trial functions, careful consideration must be given to this factor to accurately capture the asymmetric nature of the velocity and temperature profiles.

2 Problem Formulation

In Fig. 1, the problem investigated is shown. Fig. 1 illustrates how the frame of reference is fixed in the center. At the bottom and top walls, fluid is injected or sucked at the same speed as it passes through the plates, which are a large extent in the z-direction.

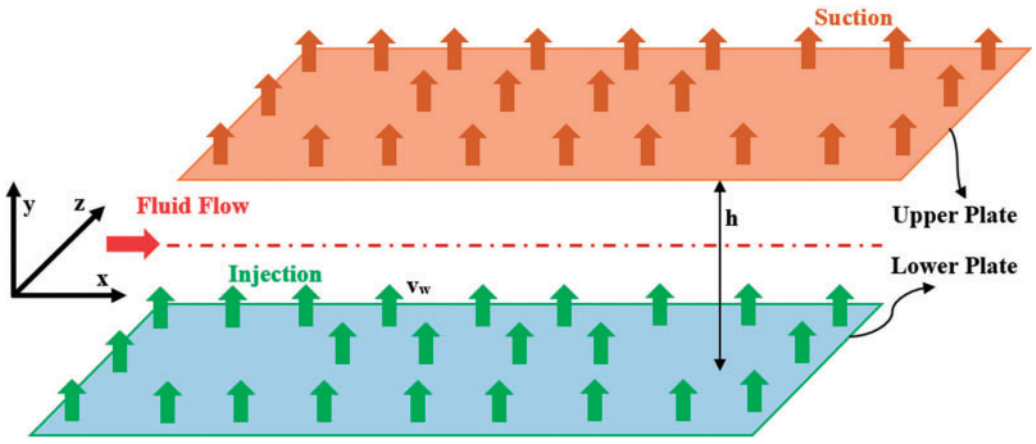

Figure 1: Third-grade fluid induced convective flow diagram across porous parallel plates

The assumptions are listed below:

- Steady, laminar, incompressible flow

- Hydro-dynamically and thermally fully developed
- Uniform suction and injection velocity
- Walls are very large along the lateral direction

The equation of continuity is as follows:

$$\nabla.\vec{V} = 0 \tag{1}$$

where, $\vec{V}$ is used to denote velocity vector. The conservation equations [9] (momentum and energy) are given below as follows:

$$\rho\frac{D\vec{V}}{Dt} = \nabla.\bar{\tau} \tag{2}$$

$$\rho c_p\frac{DT}{Dt} = k\frac{d^2T}{dy^2} + \tau L + Q\left(T - T_0\right) \tag{3}$$

where, τ represents the stress tensor, c_p denotes fluid specific heat, ρ is the fluid density, L is the velocity gradient matrix, k denotes the fluid thermal conductivity, Q is the reactant concentration [9], which measures internal heat generation and T_0 is the lower wall temperature.

The following constitutive equation describes the relationship between shear stress and strain rate for third-grade fluids:

$$\tau = -pI + \mu A_1 + \alpha_1 A_2 + \alpha_2 A_1^2 + \beta_1 A_3 + \beta_2\left(A_1A_2 + A_2A_1\right) + \beta_3\left(trA_1^2\right)A_1 \tag{4}$$

where, μ, β_1, β_2, β_3, α_1 and α_2 are properties of third-grade fluids, p denotes static pressure. These properties are estimated from experiments conducted in a rheometer. It is important to note that the constitutive relation between stress and strain rate, captured by Eq. (4) is highly non-linear in nature, which increases the complexity level of the momentum conservation equation from solution point of view. A_1, A_2 and A_3 are kinematic tensors which are obtained as follows:

$$A_1 = \left(grad\vec{V}\right) + \left(grad\vec{V}\right)^T \tag{5}$$

A_n is presented by the following equation:

$$A_n = \frac{DA_{n-1}}{Dt} + A_{n-1}\left(grad\vec{V}\right) + \left(grad\vec{V}\right)^T A_{n-1}, n = 2, 3 \tag{6}$$

For third-grade fluids, the maximum value of $n = 3$. Velocity u does not depend on the z coordinate because of the assumption of very large plate along the z-direction.

It is assumed that hydrodynamically developed (fully) is taken into consideration. Thus, the following type of velocity is looked for:

$$\vec{V} = \left[u\left(y\right), 0, 0\right] \tag{7}$$

Utilizing all assumptions and Eqs. (1)–(7), momentum conservation equations along three directions are as follows:

$$\mu\frac{d^2u}{dy^2}+6\left(\beta_2+\beta_3\right)\frac{d^2u}{dy^2}\left(\frac{du}{dy}\right)^2-\frac{\partial p}{\partial x}=\rho v\frac{du}{dy} \tag{8.1}$$

$$\left(2\alpha_1+\alpha_2\right)\frac{d}{dy}\left[\left(\frac{du}{dy}\right)^2\right]=\frac{\partial p}{\partial y} \tag{8.2}$$

$$\frac{\partial p}{\partial z}=0 \tag{8.3}$$

Energy conservation equation is given below as:

$$k\frac{d^2T}{dy^2}d+\mu\left(\frac{du}{dy}\right)^2+2\left(\beta_2+\beta_3\right)\left(\frac{du}{dy}\right)^4+Q\left(T-T_0\right)=\rho c_p v\frac{dT}{dy} \tag{9}$$

Convective term along flow direction (along x) has been neglected based on the assumption of very less temperature gradient along flow direction compared to the temperature gradient along the cross-flow direction (y direction). That means $u\frac{\partial T}{\partial x}$ has been neglected in comparison to $v\frac{\partial T}{\partial y}$. Effect of $v\frac{\partial T}{\partial y}$ has been considered in the present study which is valid when the gap between the parallel plates is small compared to the length of the plate.

Boundary conditions:

$$u\left(0\right)=u\left(h\right)=0,\ T\left(0\right)=T\left(h\right)=T_0 \tag{10.1}$$

$$v\left(0\right)=v\left(h\right)=v_w \tag{10.2}$$

Vertical velocity component, for uniform suction and injection in the small gap in the plates, is approximately considered as:

$$v\approx v_w \tag{11}$$

Eq. (8.1), therefore, reduces as follows:

$$\mu\frac{d^2u}{dy^2}+6\left(\beta_2+\beta_3\right)\frac{d^2u}{dy^2}\left(\frac{du}{dy}\right)^3-\rho v_w\frac{du}{dy}=\frac{\partial p}{\partial x} \tag{12}$$

From Eq. (8.3) it is clear that p does not depend upon z. The following equation for p is yielded from Eq. (8):

$$p=\int_0^y\left(2\alpha_1+\alpha_2\right)\frac{d}{dy}\left[\left(\frac{du}{dy}\right)^2\right]dy+f\left(x\right)+c \tag{13}$$

In Eq. (13), c represents an integral constant. It is concluded from Eq. (13) that $\frac{\partial p}{\partial x}$ is dependent on x alone and can be represented as $\frac{dp}{dx}$. Therefore, Eq. (12) is reduced to the following form:

$$\mu\frac{d^2u}{dy^2} + 6\left(\beta_2 + \beta_3\right)\frac{d^2u}{dy^2}\left(\frac{du}{dy}\right)^3 - \rho v_w\frac{du}{dy} = \frac{dp}{dx} \tag{14}$$

In Eq. (14), some properties like α_1, α_2 and β_3 do not appear. The reason is attributed to the vanishing of all terms in the corresponding kinematic tensors. This, finally, produces no term with this properties in Eq. (14) because multiplication with zero matrix results in zero.

In Eq. (14), $\frac{dp}{dx}$ depends on x. u is a function of y alone making the left hand side of Eq. (14) depending on y only. This means both sides of Eq. (14) are separately equal to a constant. Governing equations are made dimensionless by the following:

$$\begin{aligned} &y^* = \frac{y}{h}, u^* = \frac{u}{U_0}, A = \left[\frac{\left(\beta_2 + \beta_3\right)U_0^2}{\mu h^2}\right], \mathrm{Re} = \frac{\rho v_w h}{\mu}, N = \frac{dp}{dx}\frac{h^2}{\mu U_0}, \theta = \frac{T - T_0}{T_0}, \\ &Br = \frac{\mu U_0^2}{kT_0}, Pe = \frac{\rho c_p v_w h}{k}, N_1 = \frac{Qh^2}{k} \end{aligned} \tag{15}$$

where, y^* is the dimensionless y coordinate; u^* represents the dimensionless velocity along the x direction. Re represents the cross-flow Reynolds number on the basis of uniform suction/injection velocity. For higher velocity of suction and injection, cross-flow Re increase. Re = 0 signifies the case for flow through impermeable/non-porous boundaries. A is the third-grade fluid parameter, θ represents the dimensionless temperature, Br is the Brinkman number and Pe represents Peclet number, and N is the dimensionless pressure gradient. A signifies the effect of the non-Newtonian characteristics of the fluid. A = 0 retrieves the Newtonian fluid flow case. Br captures the relative significance of viscous dissipation in flow. Pe represents the relative strength of cross flow convection compared to the conductive heat transfer. N_1 represents heat source parameter. Higher values of N_1 signify more internal heat generation. The reference velocity U_0 is obtained as follows:

$$U_0 = -\left(\frac{dp}{dx}\right)\frac{h^2}{\mu} \tag{16}$$

Consequently, N is obtained as follows:

$$N = -1 \tag{17}$$

Asterisks have been omitted from the dimensionless variables for convenience and the following dimensionless governing equations and boundary conditions are obtained:

$$\frac{d^2u}{dy^2} + 6A\frac{d^2u}{dy^2}\left(\frac{du}{dy}\right)^2 + N = \mathrm{Re}\frac{du}{dy} \tag{18.1}$$

$$\frac{d^2\theta}{dy^2} + Br\left(\frac{du}{dy}\right)^2 + 2ABr\left(\frac{du}{dy}\right)^4 + N_1\theta = Pe\frac{d\theta}{dy} \tag{18.2}$$

Dimensionless boundary conditions:

$$u(0) = u(1) = 0 \tag{19.1}$$

$$\theta(0) = \theta(1) = 0 \tag{19.2}$$

3 Solution

3.1 Solution by LSM

Eqs. (18.1) and (18.2) are non-linear which may not admit analytical solutions. In the current study, LSM is utilized to get solution of Eqs. (18.1) and (18.2). First, base functions/trial functions need to be chosen for application of LSM. The base functions need to be selected with careful consideration due to non-symmetry of velocity distribution. With rise in cross-flow Reynolds number, velocity profile gets distorted. In view of this, the approximations for temperature and velocity profiles are made as a combining both symmetric and asymmetric trial functions. All the trial/base functions are so chosen that they will satisfy the boundary conditions given by Eqs. (19.1) and (19.2). In consideration of this, the approximate equations are picked up as follows:

$$u = c_1 y^2 (1-y) + c_2 y^3 (1-y) + c_3 y (1-y) \tag{20.1}$$

$$\theta = c_4 y^2 (1-y) + c_5 y^3 (1-y) + c_6 y (1-y) \tag{20.2}$$

Upon substitution of Eqs. (20.1) and (20.2) in Eqs. (18.1) and (18.2) residual functions are resulted as follows:

$$R_1 = \frac{d^2u}{dy^2} + 6A\frac{d^2u}{dy^2}\left(\frac{du}{dy}\right)^2 + N - \mathrm{Re}\frac{du}{dy} \tag{21}$$

$$R_2 = \frac{d^2\theta}{dy^2} + Br\left(\frac{du}{dy}\right)^2 + 2ABr\left(\frac{du}{dy}\right)^4 + N_1\theta - Pe\frac{d\theta}{dy} \tag{22}$$

Symbolic computation of MATLAB is utilized for carrying the steps. Upon substitution of the approximated velocity from Eq. (20.1) into Eq. (21), the following equations is yielded:

$$\begin{aligned} R_1 = {} & c_1(2-6y) + c_2\left(6y-12y^2\right) - 2c_3 + 6A\left[c_1(2-6y) + c_2\left(6y-12y^2\right) - 2c_3\right] \\ & \left[c_1\left(2y-3y^2\right) + c_2\left(3y^2-4y^3\right) + c_3(1-2y)\right]^2 + N - \mathrm{Re}\left[c_1\left(2y-3y^2\right) + c_2\left(3y^2-4y^3\right) + c_3(1-2y)\right] \end{aligned} \tag{23}$$

$$\begin{aligned} R_2 = {} & c_4(2-6y) + c_5\left(6y-12y^2\right) - 2c_6 + Br\left[c_1\left(2y-3y^2\right) + c_2\left(3y^2-4y^3\right) + c_3(1-2y)\right]^2 \\ & +2ABr\left[c_1\left(2y-3y^2\right) + c_2\left(3y^2-4y^3\right) + c_3(1-2y)\right]^2 + N_1\left[c_4y^2(1-y) + c_5y^3(1-y) + c_6y(1-y)\right] \\ & -Pe\left[c_4\left(2y-3y^2\right) + c_5\left(3y^2-4y^3\right) + c_6(1-2y)\right] \end{aligned} \tag{24}$$

Summation of square of residuals R_1 and R_2 are determined as follows:

$$S_1 = \int_0^1 R_1^2 dy \tag{25.1}$$

$$S_2 = \int_0^1 R_2^2 dy \tag{25.2}$$

S_1 and S_2 are to be minimized with respect to the unknowns c_1, c_2, c_3 and c_4, c_5, c_6, respectively. In this process, three non-linear coupled algebraic equations will be generated for the unknowns c_1, c_2 c_3 and the same number of coupled, non-linear algebraic equations will be generated for c_4, c_5, c_6. The equations are generated as follows:

$$\frac{\partial S_1}{\partial c_1} = \frac{\partial}{\partial c_1}\left(\int_0^1 R_1^2 dy\right) = \int_0^1 R_1 \frac{\partial R_1}{\partial c_1} dy = 0 \tag{26.1}$$

$$\frac{\partial S_1}{\partial c_2} = \frac{\partial}{\partial c_2}\left(\int_0^1 R_1^2 dy\right) = \int_0^1 R_1 \frac{\partial R_1}{\partial c_2} dy = 0 \tag{26.2}$$

$$\frac{\partial S_1}{\partial c_3} = \frac{\partial}{\partial c_3}\left(\int_0^1 R_1^2 dy\right) = \int_0^1 R_1 \frac{\partial R_1}{\partial c_3} dy = 0 \tag{26.3}$$

$$\frac{\partial S_2}{\partial c_4} = \frac{\partial}{\partial c_4}\left(\int_0^1 R_2^2 dy\right) = \int_0^1 R_2 \frac{\partial R_2}{\partial c_4} dy = 0 \tag{27.1}$$

$$\frac{\partial S_2}{\partial c_5} = \frac{\partial}{\partial c_5}\left(\int_0^1 R_2^2 dy\right) = \int_0^1 R_2 \frac{\partial R_2}{\partial c_5} dy = 0 \tag{27.2}$$

$$\frac{\partial S_2}{\partial c_6} = \frac{\partial}{\partial c_6}\left(\int_0^1 R_2^2 dy\right) = \int_0^1 R_2 \frac{\partial R_2}{\partial c_6} dy = 0 \tag{27.3}$$

The non-linear system of coupled, algebraic equations given by Eqs. (26.1)–(26.3) are first solved for the unknowns c_1, c_2, and c_3. Once these are solved, then Eqs. (27.1)–(27.3) are solved using the expression for u. Equations are solved by symbolic computation.

3.2 Numerical Solution

For establishing validity of the outcomes of LSM, numerical solution by shooting method is obtained. In Eqs. (21) and (22), the following substitutions are made: $\frac{du}{dy} = B$ and $\frac{d\theta}{dy} = q$.

These substitutions result in the following system of equations:

$$\frac{dB}{dy} + 6AB^2\frac{dB}{dy} + N = \mathrm{ReB} \tag{28.1}$$

$$\frac{du}{dy} = B \tag{28.2}$$

$$\frac{dq}{dy} + BrB^2 + 2ABrB^4 + N_1\theta = (Pe)\, q \tag{28.3}$$

$$\frac{d\theta}{dy} = q \tag{28.4}$$

By these substitutions, two second order equations given by Eqs. (21) and (22), are converted to four number of 1st order equations. Eqs. (28.1)–(28.4) are solved by finite difference method coupled with shooting technique. Equations are discretized as follows:

$$\left(\frac{B_{i+1}-B_i}{\Delta y}\right)+6Az_i^2\left(\frac{B_{i+1}-B_i}{\Delta y}\right)+N=\mathrm{ReB}_i \tag{29.1}$$

where, z_i represents the z at the i-th grid point and Δy is the grid size in the y direction.

Eq. (29) leads to the following equation:

$$B_{i+1}=B_i+\Delta y\left(\frac{\mathrm{ReB}_i-N}{1+6AB_i^2}\right) \tag{29.2}$$

Eq. (28.2) is replaced by the following finite difference equation:

$$u_{i+1}=u_i+\Delta yB_i \tag{29.3}$$

Eqs. (29.2) and (29.3) are solved by shooting technique. At the 1st grid point, $u_1 = 0$. For initiating the marching procedure, z_1 is guessed. Then from Eqs. (29.2) and (29.3), iteration is repeated unless the boundary condition given by Eq. (19.1) ($u_1 = 0$) is satisfied. Once velocity at different grid points are calculated, these can be utilized for solving Eqs. (28.3) and (28.4) by the shooting technique. For initiating the iteration, q_1 is guessed and corrected unless temperature at the boundary $y = 1$, $\theta = 0$ is satisfied.

Entropy generation is given as follows:

$$E_g=\frac{K}{T_0^2}\left(\frac{dT}{dy}\right)^2+\frac{\mu}{T_0}\left(\frac{du}{dy}\right)^2\left[1+2\frac{(\beta_2+\beta_3)}{\mu}\left(\frac{du}{dy}\right)^2\right] \tag{30}$$

E_g is the entropy generation parameter. After making it dimensionless we get dimensionless entropy generation number as follows:

$$N_s=\left(\frac{d\theta}{dy}\right)^2+Br\left(\frac{du}{dy}\right)^2\left[1+2A\left(\frac{du}{dy}\right)^2\right] \tag{31}$$

where, N_s represents dimensionless entropy generation parameter. Bejan number (Be) is calculated as follows:

$$Be=\frac{\left(\frac{d\theta}{dy}\right)^2}{Ns} \tag{32}$$

Volumetric flow rate is of interest from practical consideration. As the parallel plates are large along the z direction, and these are not of any finite extent, dimensionless volumetric flow rate per unit width is calculated. The dimensionless flow rate, based on per unit width, is as follows:

$$q_1=\frac{Q_1}{b}=\int_0^1 u\,dy=\int_0^1\left[u=c_1y^2(1-y)+c_2y^3(1-y)+c_3y(1-y)\right]dy \tag{33}$$

where, Q_1 is the dimensional flow rate, q is dimensionless flow rate per unit width and b is the width of the parallel plates. Dimensionless flow rate per unit width is given below as:

$$q_1 = \frac{c_1}{12} + \frac{c_2}{20} + \frac{c_3}{6} \tag{34}$$

4 Results and Discussion

This section examines the effects of various factors on temperature, velocity, Bejan number, and entropy generation rate. In this regard, first, the range of these parameters is to be fixed. It is not easy to fix the range of various parameters using range values of their physical characteristics since experimental values of all the attributes of third-grade fluids are seldom documented in the literature. Therefore, the range of parameters is fixed from different studies for similar and nearly similar applications. Parametric values are chosen as considered by Adesanya and Makinde [13] and by Balamurugan et al. [12]. Adesanya and Makinde [13] studied flow and heat transfer in reactive third-grade fluid through a vertical channel including the buoyancy effect. Suction/injection, however, was not included. In the study of Balamurugan et al. [12] heat transfer in a Newtonian fluid with a heat generation effect, with suction/injection was studied. As the present study has some similarities with the cited works, the parameters are chosen almost in the same range as considered in these cited studies.

For heat transmission in a third-grade fluid along a vertical channel, Adesanya and Makinde's study [13] took into account the third-grade fluid parameter in the range of 0.01–0.3, and in one instance, unity. In light of this, the value of A in the current study has been chosen to fall between 0.1 and 0.4. The cross-flow Balamurugan [12] considered Reynolds number Re to be between 0.1 and 10. Re has been altered between 0 and 7 in this investigation. The maximum variation in the Peclet number was 10. Assuming a minimal temperature difference along the flow direction, the fluid utilized in the current study is third-grade fluid, and axial convection is not taken. Nonetheless, the present effort has taken cross-flow convection into account. Extremely big Pe is not taken into account in light of these variables. Instead, Pe is limited to a maximum of 1.5. In Adesanya and Makinde's [13] investigation, the heat generation parameter N_1 is altered between 0 and 1 [13]. The heat generation parameter was chosen by Balamurugan et al. [12] from 0.1 to 0.4. The heat generation parameter was chosen up to unity in the Obalalu et al. [1] investigation. N_1 was considered up to 7 in this study to examine the impact of increased heat output. Comparing the current study to previous research [12,13], greater values of Br are also taken to investigate the impact of higher Br on the field variables and entropy generation.

The results of the current investigation are compared with those of the internal numerical code in Fig. 2a. Fig. 2 displays the comparison of dimensionless velocity distribution obtained from LSM and Numerical methods for $A = 0.2$, $N_1 = 2$, $Br = 2$, $Pe = 1$ and $Re = 3$. It is observed that both results match well. The maximum velocity occurs at nearly $y = 0.6$ for both numerical and LSM results. As $Re = 3$, the velocity profile is distorted and the peak velocity shifts towards $y = 0.6$. In Fig. 2c also, dimensionless velocity distribution from LSM and numerical methods are compared for a different set of parameters ($A = 0.3$, $N_1 = 3$, $Br = 3$, $Pe = 1.5$, $Re = 6$). The results match well. Similar comparisons are made for dimensionless temperature distribution for two different sets of parameters, as shown in Fig. 2c,d and they are observed to be in close agreement The results of the current study are compared with those of Danish et al. [30] in Fig. 2e. Their investigation yields an exact analytical solution for velocity distribution. The velocity distribution of Danish et al. [30] for the limiting case of $Re = 0$ is compared with the results of the current investigation. The findings are found to be highly consistent, confirming the accuracy of the data.

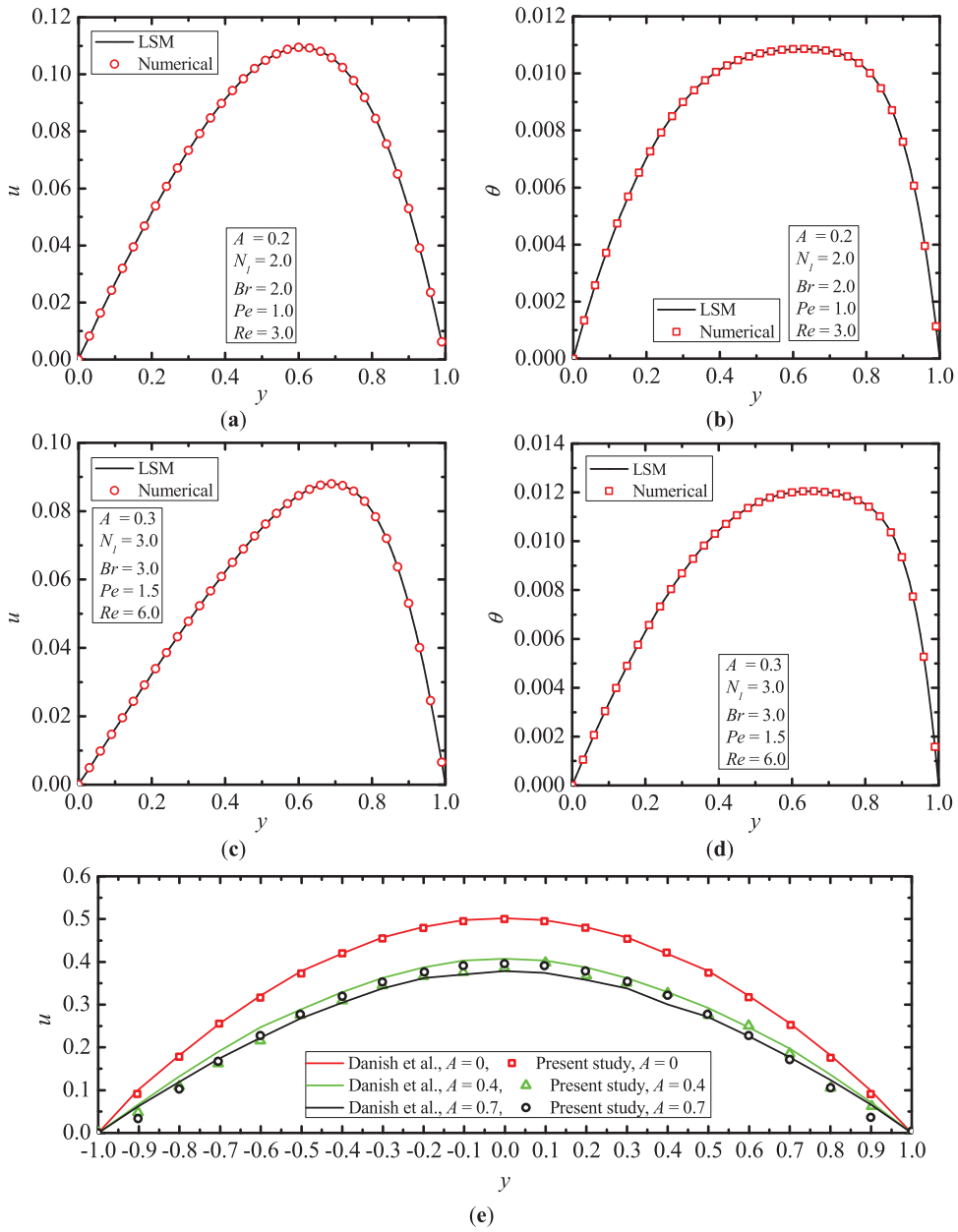

Figure 2: Comparison of results from LSM and Numerical method **(a)** variation of velocity with y when A = 0.2, **(b)** variation of temperature with y when A = 0.2, **(c)** variation of velocity with y when A = 0.3, and **(d)** variation of temperature with y when A = 0.2, and **(e)** validation of present result with Danish et al. [30] for various A

Fig. 3a presents the effects of A on velocity distribution with y. It is observed that with an increase in A, the resistance toward flow is greater. This leads to lower velocity with the rise in A. The impacts of cross-flow Re on velocity are shown graphically in Fig. 3b. It is clear from the graph that with a rise in Re (signifying an increment in injection velocity at the lower wall and a rise in suction at the upper wall), the velocity profile is shifted towards the right breaking the symmetric nature of it. Furthermore, in addition to shifting the velocity profile towards the upper wall, the maximum velocity also reduces. This is attributed to the higher resistance offered when the injection velocity is increased.

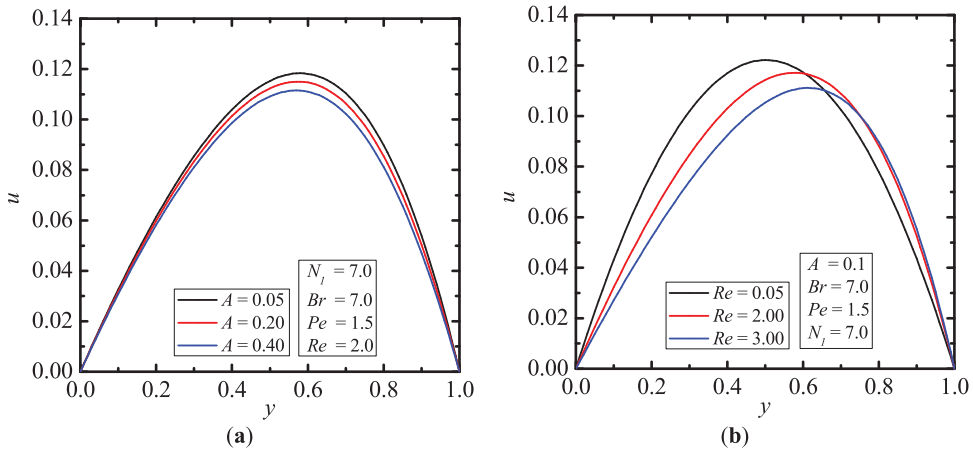

Figure 3: **(a)** Impact of A on velocity distribution and **(b)** impact of Re on distribution

Fig. 4a depicts the influence of A on the temperature profile. It is found that temperature also displays a non-symmetric pattern as revealed by the velocity profile. But injection reduces heat transfer, whereas suction causes enhancement of heat transfer. From the aspect of heat transfer at the walls, if we examine temperature plots in Fig. 4a, it can be noted that for all the selected A (A = 0.05, 0.30, and 0.40), the velocity gradient is lower near the lower wall compared to the velocity gradient near the upper wall. For the same A, therefore, heat transfer from the upper wall is higher than the lower wall for the same A. Further, an increment in A reduces the heat transfer from the upper wall as it causes a reduction in the temperature of the fluid as a whole. Reduction in A causes lower velocity, causing a lower velocity gradient in general. Thus, viscous heating contributes less to the rise in temperature. In addition to this, with the rise in Re, cross-convective heat transport increases. This results in more energy transport from the lower wall towards the upper and higher temperature near the upper wall. It can be observed that at a distance of 0.1 from the lower wall, dimensionless temperature (which represents excess temperature compared to the wall temperature) is around 0.3; whereas, at a distance of 0.1 from the right wall, temperature is around 0.45. The influence of Re is more prominent on temperature compared to the effect of A. Fig. 4b indicates that with an upturn in Re from 0.05 to 3, maximum velocity decreases from 0.13 to 0.10. Again for Re = 3, at y = 0.2 from the lower wall, the dimensionless temperature is observed to be 0.04. At the same location from the upper wall, the dimensionless temperature is 0.09. This is the result of higher cross-flow convective heat transport. Another important point is the reduction in temperature in a section with an increase in Re. This is attributed to lower axial velocity causing less velocity gradient and consequently less viscous heating. The effect of Pe on temperature is depicted in Fig. 4c. The correct number of the current investigation is considered on uniform suction/injection velocity. Therefore, Pe is a measure of the cross-convective heat transport compared to the conductive heat transport. With an increase in Pe, temperature is reduced adjacent to the lower wall, whereas temperature rises with Pe near the right wall. Higher values of Pe signify more cross-flow convective heat transport. Therefore, dimensionless temperature decreases near the lower wall. Due to higher cross-convective heat transport, the temperature near the upper wall increases. At y = 0.2, the dimensionless temperature for Pe = 0.05 is around 0.09, and for Pe = 1.5, the temperature decreases to nearly 0.06. At the symmetric position of 0.2 from the upper wall, for Pe = 0.05, the dimensionless temperature is 0.011. When Pe rises to 1.5, dimensionless temperature escalates to 0.012.

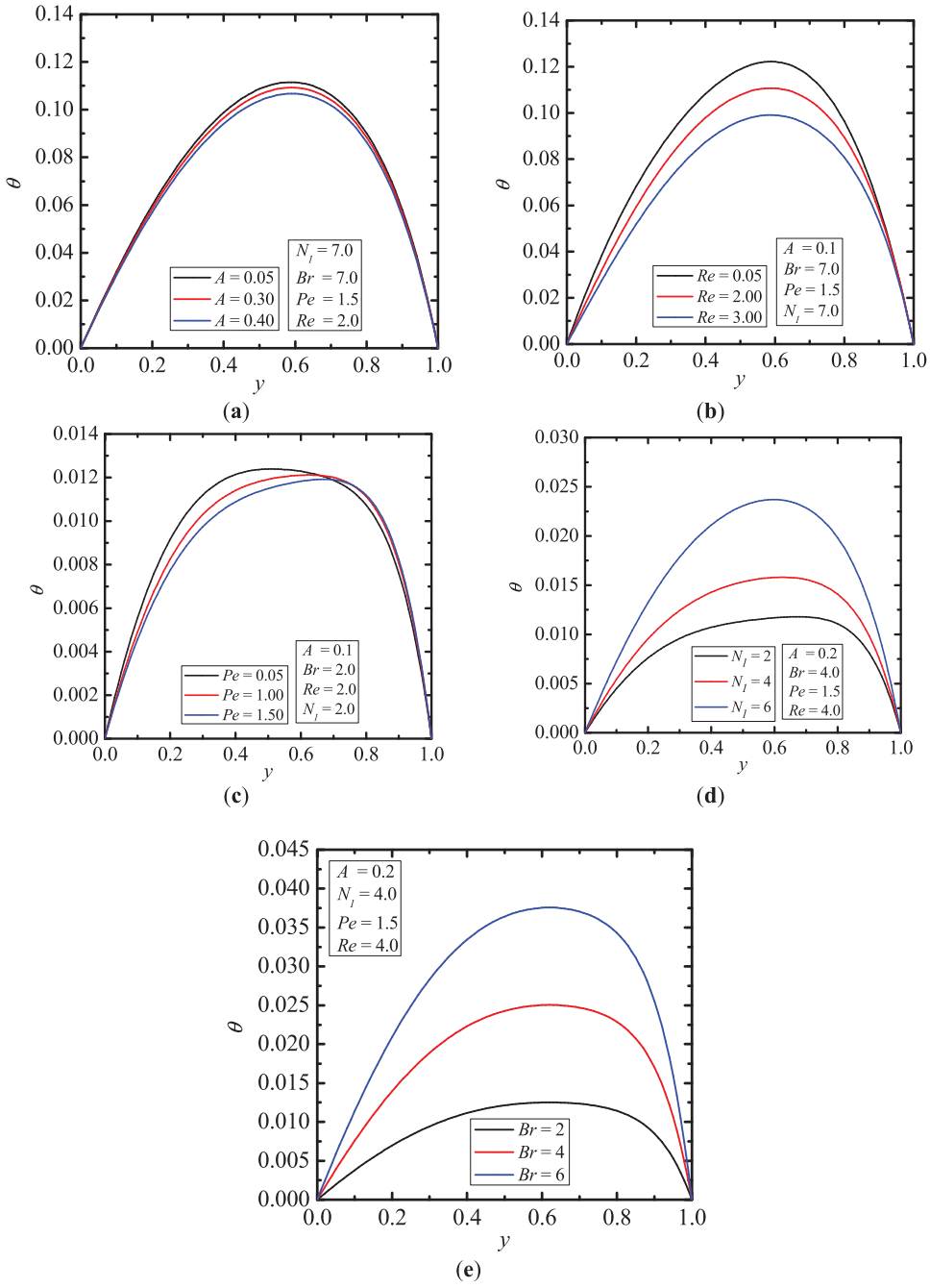

Figure 4: **(a)** Impact of A on temperature; **(b)** Impact of Re on temperature; **(c)** Impact of Pe on temperature; **(d)** Impact of N_1 on temperature; **(e)** Impact of Br on temperature

The impact of the heat generation parameter N_1 on temperature is shown in Fig. 4d. The first characteristic to be observed is the non-symmetric nature of the temperature profile even for small N_1 = 0.05. This trend is attributed to the injection/suction of the fluid in the porous walls. Another feature is the rise in temperature with rise in heat generation parameter. As the heat generation parameter rises, fluid temperature upturns. This causes an increase in the slope at the walls, leading to the enhancement in wall heat transfer. This means, to maintain the walls at constant temperatures, more heat has to be transferred from the walls to

the surrounding coolant. The effect of *Br* on temperature is displayed in Fig. 4e. The impact of *Br* is similar to that of the heat generation parameter because *Br* plays the role similar to a heat source. Therefore, with a rise in *Br*, the temperature of the fluid increases.

Fig. 5a depicts the influence of non-Newtonian material parameters on the entropy generation. Without the effect of suction/injection, the entropy generation plot, for a different non-Newtonian parameter, is symmetric about the central line $y = 0.5$. In the present study, N_s is non-symmetric and minimum at the central line of the plates. N_s drops at the injection wall and upturns at the suction wall. This feature is due to the increased friction effect near the suction boundary compared to the injection wall. It is noted that the effect of A on N_s is marginal in the entire domain except near the suction wall. This is attributed to the increased friction at the suction wall. The effect of the relative importance of irreversibility due to temperature gradient effect on total entropy is shown in Fig. 5a. It is noted that *Be* increases near the center and in all other regions, it is less than a value of unity. For $A = 0.20$, *Be* reaches nearly unity at $y = 0.6$. However, in other regions ($0 < y < 0.4$, $0.6 < y < 1$), *Be* is only 0.10. This is attributed to higher frictional resistance near the walls which leads to more entropy generation. Compared to this, entropy generation due to temperature gradient is low. Near the central region ($0.4 < y < 0.6$), the velocity gradient is very less leading to almost no entropy generation there. At this region, entropy generation is only because of the temperature gradient effect. It is observed from Fig. 5b that at $y = 0.6$, Bejan number $Be = 0$ indicating no entropy generation at this point. This point of no entropy generation occurs at the centre $y = 0$ when the velocity profile is symmetric. For the distorted velocity profile for suction/injection, this point is shifted to $y = 0.6$.

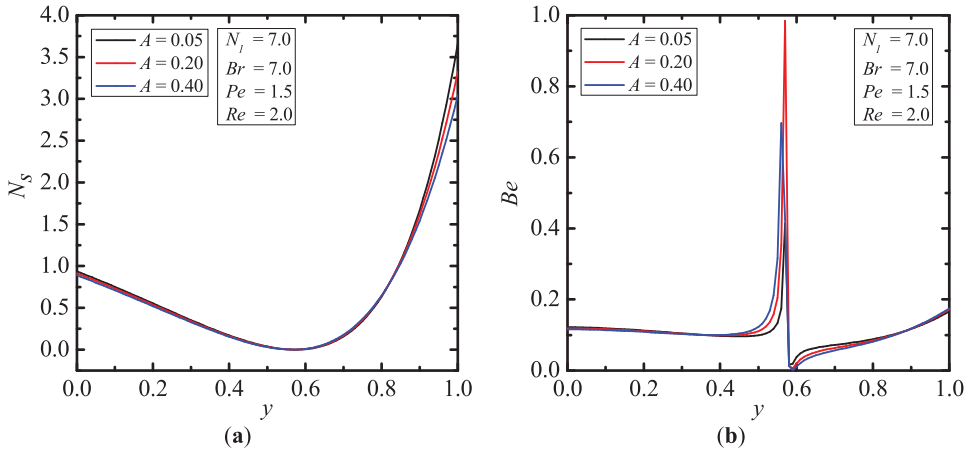

Figure 5: **(a)** Effect of third-grade parameter (A) on entropy generation, and **(b)** effect of third-grade fluid parameter (A) on Bejan number

The effects of Reynolds number on entropy generation (N_s) and *Be* are illustrated in Fig. 6a and b, respectively. For $Re = 0.05$, N_s is nearly symmetric and attains its minimum value at the center. Furthermore, N_s is maximum at the walls and achieves a minimum value at the center. This happened due to the symmetric velocity and temperature profile observed at the center for $Re = 0.05$. For higher values of cross-flow Reynolds number, N_s at the suction wall becomes greater and decreases at the injection wall. This phenomenon is due to the increase in frictional effects near the suction wall as a rise in suction velocity. The influence of *Re* on *Be* is shown in Fig. 6b. It is observed that for $Re = 0.05$, Be reaches a value of nearly 1 at $y = 0.5$. For $Re = 2$, the maximum value of *Be* is 0.8 and for $Re = 3$, *Be* again shows an increasing trend.

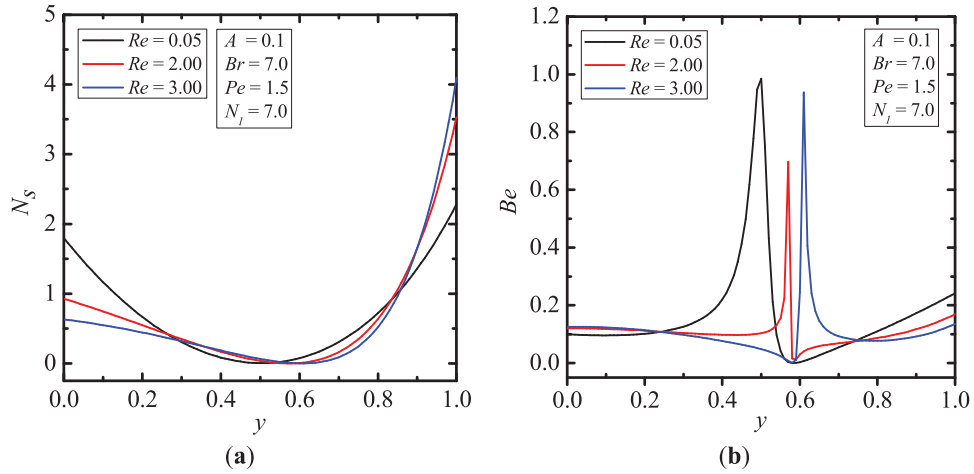

Figure 6: **(a)** Effect of *Re* on entropy generation, and **(b)** effect of *Re* on Bejan number

The effect of *Pe* on N_s and *Be* is minimal as shown in Fig. 7a and b, respectively. The momentum and energy conservation equations are uncoupled (as temperature-dependent properties are not considered). Consequently, changes in *Pe* do not affect the velocity profile. Moreover, the impact of *Pe* on temperature gradient is also marginal. Therefore, Both N_s and *Be* remain unaffected by changes in *Pe*.

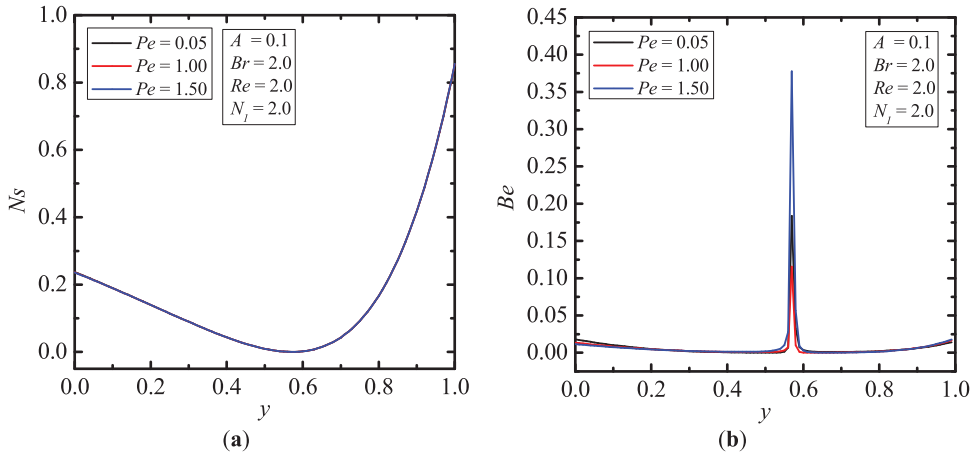

Figure 7: **(a)** Effect of *Pe* on entropy generation, and **(b)** effect of *Pe* on Bejan number

The impact of heat generation parameter N_1 on entropy generation and Bejan number are presented in Fig. 8a and b, respectively. The velocity profile is completely unaffected by N_1. Furthermore, with an increase in N_1, Bejan number increases. Also, with rise in N_1 from 2 to 6, *Be* near the center increases from nearly 0.1 to 0.6. This indicates that entropy generation due to temperature gradient is more at higher heat generation.

The effect of *Br* on entropy generation is significant as shown in Fig. 9a. With an increase in *Br*, the entropy generation in both walls increases. Again, with a rise in *Br*, *Be* also rises at the walls and the center up to 0.15 as depicted in Fig. 9b.

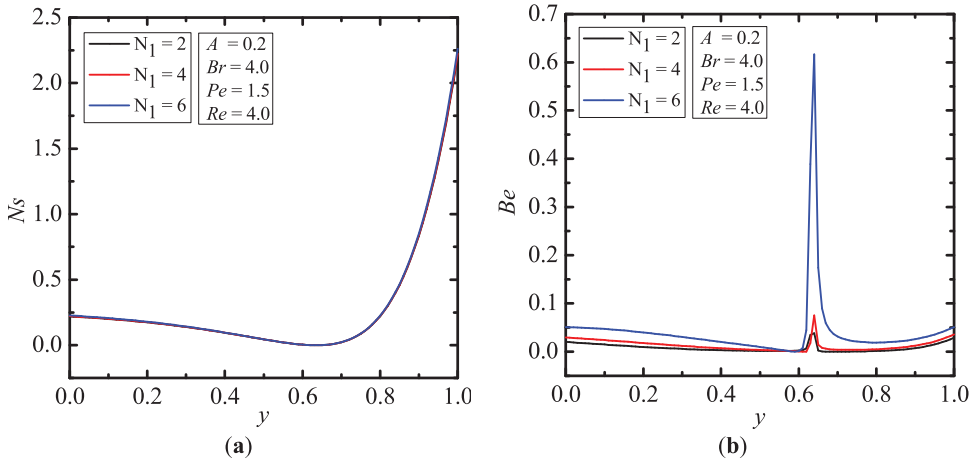

Figure 8: **(a)** Impact of N_1 on entropy generation, and **(b)** impact of N_1 on Bejan number

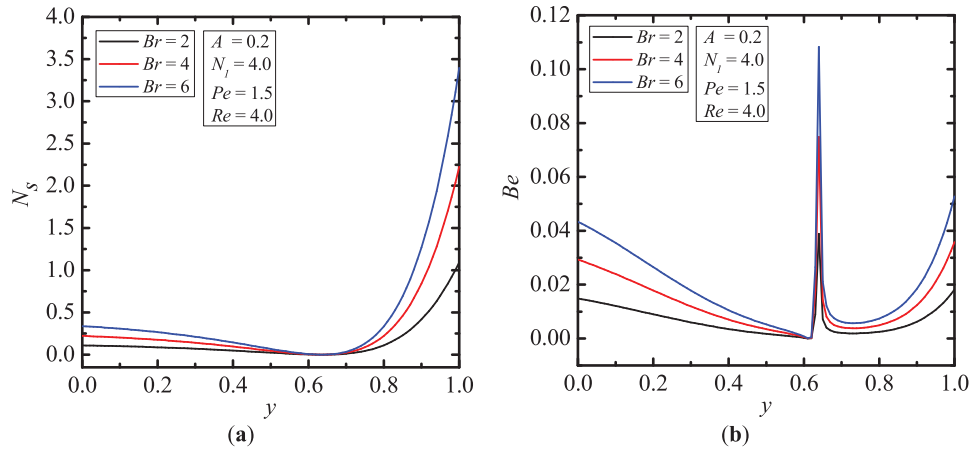

Figure 9: **(a)** Effect of *Br* on entropy generation, and **(b)** effect of *Br* on Bejan number

Fig. 10 presents how *A* affects the dimensionless flow rate for different *Re* when other parameters are fixed. With an increase in *A*, velocity reduces as a result of higher flow resistance. Consequently, the flow rate decreases. When the cross-flow Reynolds number rises, flow resistance is more with a consequent reduction in flow rate.

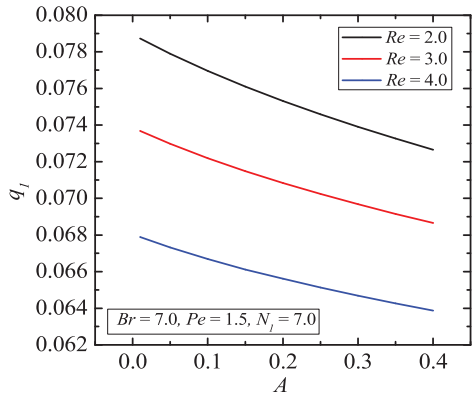

Figure 10: Effect of *Re* on dimensionless flow rate for different *A*

5 Conclusion

Large parallel permeable plates with uniform wall suction and injection are considered to study forced convective heat transfer in a reactive third-grade fluid. The LSM is used to get semi-analytical results for temperature and dimensionless velocity. To validate the LSM results, numerical solutions are also obtained.

The following important observations are made from this study:

- The velocity and temperature profiles across the plates are strongly influenced by the third-grade fluid parameter A. Temperature and velocity drop when this non-Newtonian parameter increases. Furthermore, a rise in A also arrests the non-symmetric aspect of temperature and velocity.
- Entropy generation reduces near the suction wall due to an increase in A. An increase in A reduces Be near the central region.
- An increase in cross-flow Re, causes a significant reduction in velocity and thus temperature. Also, a rise in suction/injection velocity offers higher flow resistance with a consequent decrease in axial velocity and resulting temperature.
- An increase in cross-flow Re results in an increase in entropy generation near the suction wall and the reverse obtained at the injection wall.
- Higher values of Pe cause an increase in cross-flow convective transport of energy with a consequent increase in temperature near the suction wall. More energy is convected from the injection wall causing a decrease in temperature there.
- The effect of Pe on entropy generation and Bejan number is very marginal. This may be attributed to very little velocity and temperature gradient change by any alteration in Pe.
- The effects of heat generation parameter N_1 on entropy generation and Be are small.
- Brinkman number has the strongest effect on temperature profile, N_s, and Be. An increase in Br causes an increase in N_s near both the suction and injection walls.
- Flow rate reduces significantly with an increase in A and Re.
- For solving the non-linear differential equations, the effectiveness of LSM has been established. This method can generate reasonably accurate results for non-linear equations.

In the present study, the effects of temperature-dependent properties are not considered. This consideration like the temperature-dependent density effect will produce coupled differential equations, which will be more challenging to solve. Further, the magneto-hydrodynamics effect can be included by considering an externally imposing magnetic field.

Acknowledgement: Not applicable.

Funding Statement: The authors received no specific funding for this study.

Author Contributions: The authors confirm contribution to the paper as follows: Conceptualization, Rajiva Lochan Mohanty and Sumanta Chaudhuri; methodology, Rajiva Lochan Mohanty; software, Sumanta Chaudhuri; validation, Rajiva Lochan Mohanty and Sumanta Chaudhuri; formal analysis, Anish Pandey; investigation, Rajiva Lochan Mohanty; resources, Sumanta Chaudhuri; data curation, Sumanta Chaudhuri; writing—original draft preparation, Rajiva Lochan Mohanty; writing—review and editing, Sumanta Chaudhuri and Anish Pandey; visualization, Rajiva Lochan Mohanty; supervision, Sumanta Chaudhuri. All authors reviewed the results and approved the final version of the manuscript.

Availability of Data and Materials: Not applicable.

Ethics Approval: Not applicable.

Conflicts of Interest: The authors declare no conflicts of interest to report regarding the present study.

Nomenclature

A	Third-grade fluid parameter
A_1, A_2, A_3, A_n	Matrices required for stress and strain rate (s^{-1})
B	Velocity gradient (Dimensionless)
Be	Bejan number
C	Nm^{-3}
c_1–c_6	Constants (Dimensionless)
Br	Brinkman number (Dimensionless)
c_p	Specific heat of the fluid (J kg^{-1} K)
E	Entropy generation parameter
h	Gap between the parallel plates (m)
k	Thermal conductivity of the fluid (W m^{-1} K^{-1})
L	Velocity gradient (s^{-1})
N	Pressure gradient (Dimensionless)
N_1	Heat source parameter (Dimensionless)
N_s	Dimensionless entropy generation number
p	Static pressure (Nm^{-2})
Pe	Peclect number (Dimensionless)
Q	Reactant concentration (W m^{-3} K^{-1})
q	Temperature gradient (Dimensionless)
Q_1	Volumetric flow rate (m^3 s^{-1})
q_1	Flow rate (Dimensionless)
R_1, R_2	Residual functions (Dimensionless)
Re	Cross-flow Reynolds number (Dimensionless)
S_1, S_2	Sums of the square of the residuals over the entire domain
t	Time (s)
T_0	Temperature of the walls (K)
U_0	Reference velocity (ms^{-1})
u	x component of velocity (ms^{-1})
$u^\star$	Dimensionless velocity along the axial direction
V	Velocity vector (ms^{-1})
v	y component of velocity (ms^{-1})
v_w	Velocity of suction/injection (ms^{-1})
x	Coordinate along the flow direction (m)
y	Coordinate perpendicular to the flow direction (m)
$y^\star$	Dimensionless y coordinate
z	Dimensional coordinate along lateral direction

Greek Symbols

α_1, α_2	Material parameter (N s^2 m^{-2})
β_2, β_3	Material parameters (N s^3 m^{-2})
μ	Material parameter (Ns m^{-2})
ρ	Density of the fluid (kg m^{-3})
τ	Stress tensor (N m^{-2})
θ	Dimensionless temperature of the fluid

References

1. Dehghan M, Rahmani Y, Ganji DD, Saedodin S, Valipour MS, Rashidi S. Convection-radiation heat transfer in solar heat exchangers filled with a porous medium: homotopy perturbation method versus numerical analysis. Renew Energy. 2015;74(1):448–55. doi:10.1016/j.renene.2014.08.044.
2. Ishak A, Nazar R, Pop I. Uniform suction/blowing effect on flow and heat transfer due to a stretching cylinder. Appl Math Model. 2008;32(10):2059–66. doi:10.1016/j.apm.2007.06.036.
3. Jha BK, Samaila G. Mixed convection flow from a convectively heated vertical porous plate with combined effects of suction/injection, internal heat generation and nonlinear thermal radiation. Proc Inst Mech Eng Part E J Process Mech Eng. 2023;237(4):1192–201. doi:10.1177/09544089221116963.
4. Jha BK, Aina B. Role of suction/injection on steady fully developed mixed convection flow in a vertical parallel plate microchannel. Ain Shams Eng J. 2018;9(4):747–55. doi:10.1016/j.asej.2016.05.001.
5. Aly A, Chamkha AJ, Raizah ZA. Radiation and chemical reaction effects on unsteady coupled heat and mass transfer by free convection from a vertical plate embedded in a porous medium. J Heat Mass Transf Res. 2020;7(2):95–103. doi:10.22075/jhmtr.2019.10763.1149.
6. Mollamahdi M, Abbaszadeh M, Sheikhzadeh GA. Flow field and heat transfer in a channel with a permeable wall filled with Al_2O_3-Cu/water micropolar hybrid nanofluid, effects of chemical reaction and magnetic field. J Heat Mass Transf Res. 2016;3(2):101–14. doi:10.22075/jhmtr.2016.447.
7. Sheremet MA, Roşca NC, Roşca AV, Pop I. Mixed convection heat transfer in a square porous cavity filled with a nanofluid with suction/injection effect. Comput Math Appl. 2018;76(11–12):2665–77. doi:10.1016/j.camwa.2018.08.069.
8. Das S, Jana RN, Makinde OD. MHD flow of Cu-Al_2O_3/water hybrid nanofluid in porous channel: analysis of entropy generation. Defect Diffus Forum. 2017;377:42–61. doi:10.4028/www.scientific.net/ddf.377.42.
9. Chamkha AJ, Mohamed RA, Ahmed SE. Unsteady MHD natural convection from a heated vertical porous plate in a micropolar fluid with Joule heating, chemical reaction and radiation effects. Meccanica. 2011;46(2):399–411. doi:10.1007/s11012-010-9321-0.
10. Chamkha AJ. On laminar hydromagnetic mixed convection flow in a vertical channel with symmetric and asymmetric wall heating conditions. Int J Heat Mass Transf. 2002;45(12):2509–25. doi:10.1016/S0017-9310(01)00342-8.
11. Sudhakar M, Balamurugan KS. Entropy generation analysis in a vertical porous channel with navier slip in the presence of viscous dissipation and heat source. Int J Mech Prod Eng Res Dev. 2018;8(5):261–70. doi:10.24247/ijmperdoct201829.
12. Balamurugan KS, Varma NU, Prasad JLR. Entropy generation analysis on forced and free convection flow in a vertical porous channel with aligned magnetic field and Navier slip. Heat Transf. 2023;52(7):4619–39. doi:10.1002/htj.22897.
13. Adesanya SO, Makinde OD. Thermodynamic analysis for a third grade fluid through a vertical channel with internal heat generation. J Hydrodyn. 2015;27(2):264–72. doi:10.1016/S1001-6058(15)60481-4.
14. Das S, Mahato N, Ali A, Jana RN. Thermal magneto-convection of GO-MoS_2/WEG within a heated channel retaining an aura of inclined magnetic force along with Hall currents. Heat Transf. 2022;51(6):5228–61. doi:10.1002/htj.22545.
15. Makinde OD, Eegunjobi AS. MHD couple stress nanofluid flow in a permeable wall channel with entropy generation and nonlinear radiative heat. J Therm Sci Technol. 2017;12(2):JTST0033. doi:10.1299/jtst.2017jtst0033.
16. Aris A, Amrani K, Mokhefi A, Valdiserri P, di Schio ER, Bouzit M, et al. Numerical investigation of the influence of a magnetic field on the laminar flow of a yield-stress nanofluid over a backward facing step. Front Heat Mass Transf. 2025;23(1):185–206. doi:10.32604/fhmt.2025.059833.
17. Tavares SMO, Pereira AMB, Sousa ACM, Sundar LS. Evaluating effect of magnetic field on nusselt number and friction factor of Fe_3O_4-TiO_2/water nanofluids in heat-sink using artificial intelligence techniques. Front Heat Mass Transf. 2025;23(1):131–62. doi:10.32604/fhmt.2025.055854.

18. Makaoui A, Moussaoui MA, Mezrhab A, Lahmer EB, Benhamou J. Thermal assessment of a differentially heated nanofluid-filled cavity containing an obstacle. Front Heat Mass Transf. 2025;23(1):207–30. doi:10.32604/fhmt.2024.060166.
19. Hakeem AK, Govindaraju M, Ganga B. Influence of inclined Lorentz forces on entropy generation analysis for viscoelastic fluid over a stretching sheet with nonlinear thermal radiation and heat source/sink. J Heat Mass Transf Res. 2019;6(1):1–10. doi:10.22075/jhmtr.2018.13611.1198.
20. Makinde OD, Eegunjobi AS. Entropy analysis of thermally radiating magnetohydrodynamic slip flow of casson fluid in a microchannel filled with saturated porous media. J Por Media. 2016;19(9):799–810. doi:10.1615/jpormedia.v19.i9.40.
21. Eegunjobi AS, Makinde OD. MHD mixed convection slip flow of radiating casson fluid with entropy generation in a channel filled with porous media. Defect Diffus Forum. 2017;374:47–66. doi:10.4028/www.scientific.net/ddf.374.47.
22. Mustapha EIH, Aberdane I, Taibi M, Rtibi A, Gueraoui K. Analysis of MHD thermosolutal convection in a porous cylindrical cavity filled with a Casson nanofluid, considering soret and Dufour effects. J Heat Mass Transf Res. 2023;10(2):197–206. doi:10.22075/jhmtr.2023.30532.1439.
23. Dash GC, Ojha KL. Viscoelastic hydromagnetic flow between two porous parallel plates in the presence of sinusoidal pressure gradient. Alex Eng J. 2018;57(4):3463–71. doi:10.1016/j.aej.2017.12.011.
24. Radnia H, Nazar ARS. Temperature profile of a power-law fluid over a moving wall with arbitrary injection/suction and internal heat generation/absorption. J Heat Mass Transf Res. 2017;4(1):53–64. doi:10.22075/jhmtr.2017.519.
25. Mohanty RL, Chaudhuri S, Chakraborty P, Mishra VK, Sahu KB, Das B. Assessment of heat transfer in large parallel plates with a narrow gap maintained at a constant temperature. Heat Transf. 2023;52(7):4711–31. doi:10.1002/htj.22904.
26. Mohanty RL, Mishra VK, Chaudhuri S. Temperature-dependent viscosity effects on heat transfer characteristics of grade three fluid in electromagnetohydrodynamic flow between large parallel plates maintained at uniform temperatures. Heat Transf. 2024;53(7):3855–79. doi:10.1002/htj.23116.
27. Akbarzadeh P. Pulsatile magneto-hydrodynamic blood flows through porous blood vessels using a third grade non-Newtonian fluids model. Comput Methods Programs Biomed. 2016;126(1):3–19. doi:10.1016/j.cmpb.2015.12.016.
28. Adesanya SO, Falade JA. Thermodynamics analysis of hydromagnetic third grade fluid flow through a channel filled with porous medium. Alex Eng J. 2015;54(3):615–22. doi:10.1016/j.aej.2015.05.014.
29. Opanuga AA, Gbadeyan JA, Agboola OO, Okagbue HI. Effect of suction/injection on the entropy generation of third grade fluid with convective cooling. Defect Diffus Forum. 2018;384:21–30. doi:10.4028/www.scientific.net/ddf.384.21.
30. Danish M, Kumar S, Kumar S. Exact analytical solutions for the Poiseuille and Couette-Poiseuille flow of third grade fluid between parallel plates. Commun Nonlinear Sci Numer Simul. 2012;17(3):1089–97. doi:10.1016/j.cnsns.2011.07.037.